Scale analysis of the diurnal cycle of precipitation over Continental United States

Paloma Borque[1], Marc Berenguer[2] and Isztar Zawadzki[3]

Dept. Atmospheric and Oceanic Sciences, McGill University, Montreal, Québec, Canada

[1] paloma.borque@mail.mcgill.ca

[2] marc.berenguer@crahi.upc.edu

[3] isztar.zawadzki@mcgill.ca

1. Introduction

Rainfall initiation is related to diurnal and semidiurnal radiation forcing (e.g. Wallace 1975, Carbone et al. 2002, Surcel et al. 2010). Much of the observed warm season rainfall results from a thermodynamic response to strong diurnal cycle of land surface temperature. Therefore, over some continental regions deep convection tends to peak around local afternoon and early evening hours. However, there is regional uniqueness in the precipitation pattern that implies a connection between regional characteristics and the behaviour of the precipitation field (Wallace 1975, Carbone et al. 2002, Lee et al. 2007).

Over western US the diurnal precipitation pattern becomes well organized with a late afternoon maximum along the eastern slopes of the Rocky Mountains (Carbone et al. 2002, Ahijevych et al. 2004, among others). This mountain-initiated convection tends to propagate away, leading to the local evening maximum over the adjacent plains (Lee et al. 2007).

The daily occurrence of propagating systems has a high impact on the continental diurnal cycle of precipitation. Parker and Ahijevych (2007) found that approximately 90% of the episodes identified in the east-central US were due to propagating systems from the west. A consequence of these systems result on the transport of the diurnal cycle from west to east (Surcel et al. 2010).

The objective of this work is to study the scale dependence of the diurnal cycle and the variability of the rainfall field with the location and time of the day, with special focus on the role of the different spatial scales in such variability.

2. Data and Methodology

2.1 Radar data

NOWrad mosaics produced by the WSI Corporation were analyzed in this work. NOWrad is a three-step quality controlled product with a 15-minute temporal resolution and 2 km spatial resolution. These mosaics show the maximum reflectivity measured by any radar at each grid point at any of the 16 vertical levels.

The period analyzed in this work corresponds to the summer months (June, July and August) in the period 1996 – 2007. Each reflectivity map, Z, was converted to rainfall rate, R, by the relation, $Z = 300\ R^{1.5}$. The 15 minutes resolution data were accumulated to obtain hourly rainfall data assuming rain intensity as constant over the 15 min period.

The domain where the precipitation field was analyzed covers the region from 110W to 78W and from 32N to 45N (Fig 1).

2.2 Methodology

Haar wavelets were used in order to produce a scale decomposition of the precipitation field.

The 1-D Haar wavelet transform of a function f, is defined as:

$$W_{\lambda}(t) = \int_{-\infty}^{+\infty} f(t)\psi_{\lambda,t}(x'-t)dx' \qquad (1)$$

where λ is a scale parameter, t is the variable and ψ are the wavelet functions, which depend on λ and t,

$$\psi_{\lambda,t}(x'-t) = 2^{-\lambda/2}\psi_0\left(\frac{x'-t}{2^{\lambda}}\right) \qquad (2)$$

with,

$$\psi_0(t) = \begin{cases} 1 & 0 \le t < 1/2, \\ -1 & 1/2 \le t < 1 \\ 0 & otherwise. \end{cases} \quad (3)$$

Then, the original function can be reconstructed as:

$$f(t) = \sum_{\lambda=-\infty}^{+\infty} 2^{-\lambda} \int_{-\infty}^{+\infty} W_\lambda(t)\psi_\lambda(x'-t)dx' \quad (4)$$

The wavelet power spectrum can be defined as

$$S_\lambda = \overline{2^{-\lambda}[W_\lambda(t)]^2} \quad (5)$$

where the overbar denotes the spatial average.

Applying wavelet analysis to a 2D field extends the wavelet function to a set of 3. Each of them will take into consideration the fluctuations of the field in each direction, x, y and in both directions simultaneously.

[For more detail in wavelet analysis and its mathematical derivation see Kumar and Foufoula-Georgiou 1997 and Turner et al. 2004].

The second moment of precipitation (PP) is defined as the average of the squared values of the precipitation field over the largest domain analyzed:

$$PP(x,y,t) = \overline{P(x,y,t)^2} \quad (6)$$

where P is the precipitation field, x is longitude, y is latitude and t is time.

Finally, the relative contribution of each scale to PP was defined as the ration between the wavelet power spectrum and the second moment of precipitation, then:

$$RPP_\lambda(x,y,t) = \frac{S_\lambda(x,y,t)}{PP(x,y,t)} x100 \quad (7)$$

The importance of rainfall activity at 4, 16, 64 and 256 km was analyzed in this work by examining the behaviour of RPP at these scales.

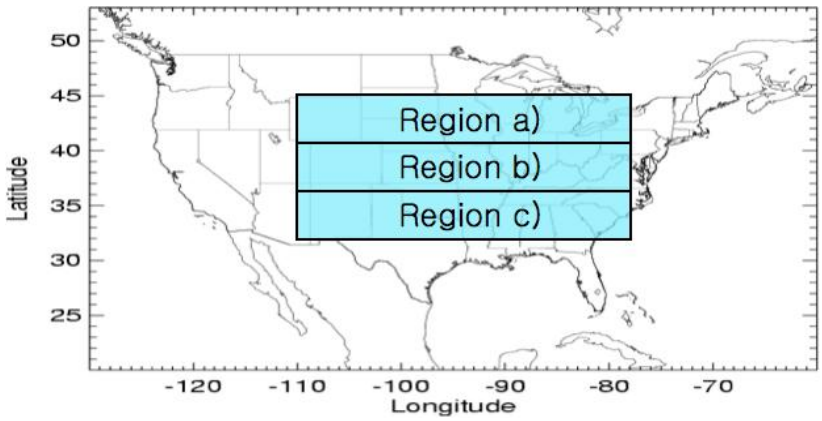

FIG. 1. Domain where the diurnal cycle of precipitation was analyzed (black rectangle) and regions where the average for the hovmöller diagrams was performed (shaded blue areas).

3. Results

3.1 Brief description of the precipitation fields over Continental United States

Figure 2 shows the latitudinally-averaged PP as a function of longitude and time of the day for the 3 domains of Fig. 1.

The beginning of light precipitation [PP below 2(mm h^{-1})^2] presents a similar slope to the solar time, indicating the relevance of the solar forcing in the initialization of the precipitant systems (Fig. 2). The importance of the solar forcing can also be seen in the maximum of rainfall activity. The maximum PP occurs at almost the same solar time over the different longitudes (Fig. 2).

Over each latitudinal band, PP around 105ºW presents high values at 00 Z. The highest value, slightly higher than 8 (mm h^{-1})^2, occurs over the central latitudes (Fig. 2b).

Immediately west of the Continental Divide (105W) precipitation tends to propagate easterly with time during

late afternoon and night hours. The velocity at which it propagates depends on latitude. Greater propagation speed is found over the central band (0.76 ° h^{-1}) and decreases both south (0.68 ° h^{-1}) and north (0.52 ° h^{-1}) from it (Fig. 2).

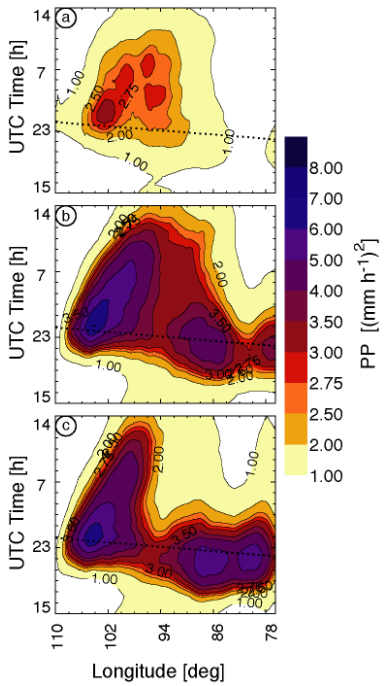

FIG. 2. Hovmöller diagrams of summer season PP average over the northern region (Fig. 1a) in the upper panel, over the central region (Fig. 1b) in the middle panel and over the southern region (Fig. 1c) in the bottom panel. The 1800 solar time is also shown in dotted black line.

The main difference between rainfall activity over the different latitudes is over the centre and eastern part of the domain. Over the southern region, PP remains stationary with time with two local maxima occurring at a similar UTC time (Fig. 2c). However over the central latitudes, the maximum PP, located around 87W, shows a slight negative tilt in the longitude-time diagram, indicative of a westward propagation with time (Fig. 2b). A completely different configuration can be seen over the northern latitudes, where two isolated PP maxima, located around 95W, does not present a clear propagation in time (Fig. 2a).

Therefore, two distinctive precipitation features can be well distinguished over continental US: an almost stationary pattern with isolated maxima located in phase with the solar forcing, and over the western boundary of the domain an eastward propagation in time of the precipitation signal (Fig. 2). This pattern is in agreement with what was found for the region by Wallace 1975, Carbone et al. 2002, Lee et al. 2007, among others.

3.2 **Importance of precipitation field at different spatial scales**

Figure 3 was computed by the latitudinal-average of RPP at each scale defined as,

$$RPP(x,t) = \frac{1}{\Delta l} \int_{l} RPP_{\lambda}(x,y,t)dl \qquad (8)$$

where, l is the latitudinal band where the average was made for each of the 3 domains shown in Fig.1.

RPP at each scale strongly depends on the time of the day and the region. In agreement with the time of rainfall activity initialization, west of 108W RPP at 4 km presents the largest value around late morning hours. The largest contribution of this scale can be found over the southern latitudes from 17 Z to 19 Z where RPP at this scale presents values higher than 27%. Over this region, the importance of this scale clearly decreases northward.

East of 100W, RPP at 4 km presents a more localized pattern with its maximum occurring at a similar solar time (Fig. 3).

Over the central longitudes RPP at this scale presents the smallest value for each latitudinal band from 01 Z until 15 Z (Figs. 3a, 3e and 3i).

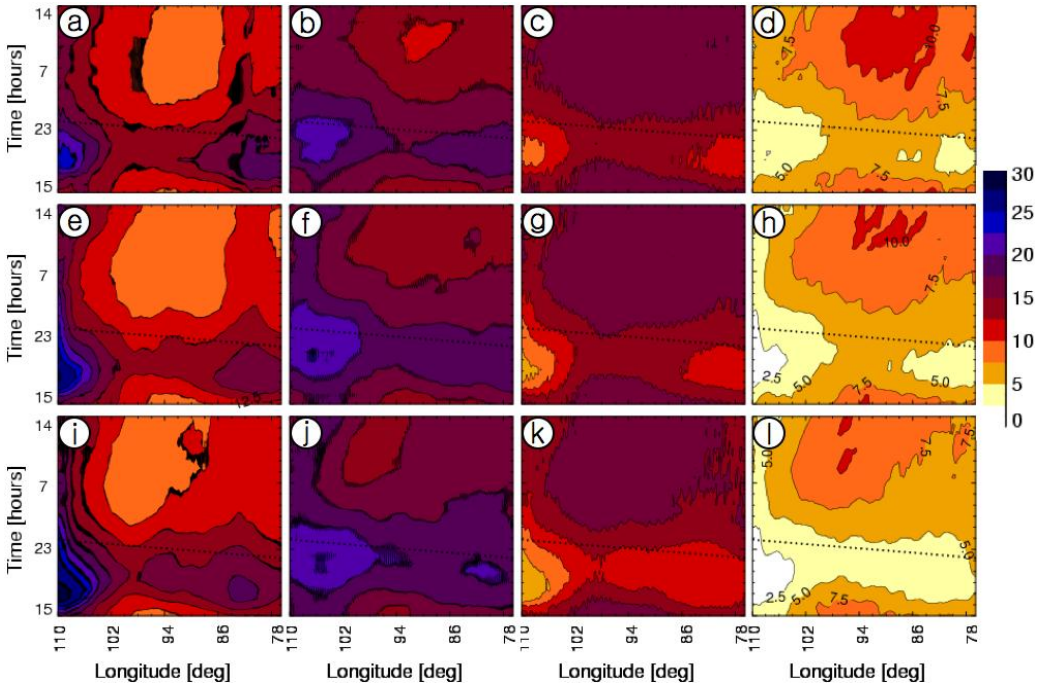

FIG. 3. Idem Fig. 2 but for RPP at 4km (left column), 16 km (central-left column), 64 km (central-right column) and 256 km (right column) for the summer.

RPP at 16 km presents some similarities with the contribution made by the 4 km scale. For example, the maximum and minimum RPP are located over similar regions and with a similar dependence with the time of the day (Figs. 3a-b, 3e-f and 3i-j). However, the maximum RPP at 16 km occurs later (at 20 Z) and further to the east (around 106W) than at 4 km.

In average, over the southern region RRP at this scale is close to 15%; however, over the northern region this amount decreases considerably representing less than 10% of the total PP (Figs. 3b and 3j). RRP at 16 km also presents a westward tilt with time during afternoon hours over each latitudinal band, in clear agreement with the solar time (Figs. 3b, 3f and 3j).

The 64 km scale shows some clear differences with the previous two scales. RPP at this scale presents its minimum value during local afternoon and its maximum during night and early morning hours (Fig. 3a-c, 3e-g and 3i-k). East of the Continental Divide, during night and morning hours rainfall activity at this scale contributes to PP by more than 15% over each latitudinal band (Figs. 3c, 3g and 3k). From 01Z to 16Z, RPP at this scale presents the highest values in connection to the nocturnal maximum of rainfall activity (Figs. 2 and 3). When and where rainfall activity at this scale becomes more important than the smaller scales depends on the latitude. Over the southern region this occurs between 102W and 94W and from 06Z to 16Z (Figs. 3j-k). Over the central latitudes, the region extends till the eastern edge of the domain and it covers from 05Z to 17Z (Figs. 3f-g). Over the northern latitudes it covers the same region but it is considerably more important over the North-Central region from 09Z to 13Z (Figs. 3b-c).

RPP at 256 km presents a similar location and time distribution as for 64 km scale. The maximum contribution of RPP at this scale occurs at night but with smaller values than at 64 km (Fig. 3). Also, the maximum RPP at 256 km occurs later in time and with a clear dependence with latitude. It is important to note that over the North-Central region RPP at this scale presents larger values than at 4 km and similar to the 16 km scale (Figs. 3a, 3b and 3d). Also, the maximum contribution of this scale is located east of 98W (Fig. 3d).

4. Summary and Conclusions

The moment at which rainfall activity at different scales contributes the most to the second moment of precipitation depends on the time of the day and the region under analysis. Also, the scale at which RPP contributes the most to the total does not remain as the most influential during the 24-hour period.

In general, the time at which the maximum contribution is achieved shifts towards later times as the scale increases. Also the region where the maximum values of RPP occur shifts eastward as the scale increases. This can be related with the smaller scales greatly influencing the onset and the maximum rainfall activity, which later on, will organize in larger rainfall patterns, mostly influenced by the bigger scales.

It is clear that there is no unique scale at which rainfall activity represents most of the total PP over the entire domain or for the 24-hour period. Over the Western and Eastern regions the time of the maximum RPP occurs

undoubtedly during local afternoon hours in connection to the smaller scales. However, over the North-Central region rainfall activity at 64 km presents the highest contribution to the total PP during night hours. This clearly shows the higher influence of the larger scales in the nocturnal precipitation regime over central US.

Finally, it is important to note that rainfall activity at the smaller scales (4 and 16 km) contributes the most to the total PP during afternoon hours whereas, the major contribution of the larger scales (64 and 256 km) mostly occurs during night and early morning hours in connection, as was previously mention, to the different stages of the precipitation life cycle.

References

Ahijevych, D.A., C.A. Davis, R.E. Carbone, and J.D. Tuttle, 2004: Initiation of Precipitation Episodes Relative to Elevated Terrain. *J. Atmos. Sci.*, **61**, 2763–2769.

Turner, B., I. Zawadski, and U. Germann, 2004: Predictability of precipitation from continental radar images. Part III: Operational nowcasting implementation (MAPLE). *J. Appl. Meteor.*, **43**:231–248

Journal of Applied Meteorology 2004 43:2, 231-248

Carbone, R.E., J.D. Tuttle, D.A. Ahijevych, and S.B. Trier, 2002: Inferences of Predictability Associated with Warm Season Precipitation Episodes. *J. Atmos. Sci.*, **59**, 2033–2056.

Kumar, P., and E. Foufoula-Georgiou, 1997: Wavelet analysis for geophysical applications. *Rev. Geophys.,* **35**, 385-412.

Kincer, J.B., 1916: Daytime and nighttime precipitation and their economic significance. *Mon. Wea. Rev.*, **44**, 628–33.

Lee, M.I., S.D. Schubert, M.J. Suarez, I.M. Held, N.C. Lau, J.J. Ploshay, A. Kumar, H.K. Kim, and J.K.E. Schemm, 2007: An Analysis of the Warm-Season Diurnal Cycle over the Continental United States and Northern Mexico in General Circulation Models. *J. Hydrometeor.*, **8**, 344–366.

Parker, M.D., and D.A. Ahijevych, 2007: Convective Episodes in the East-Central United States. *Mon. Wea. Rev.*, **135**, 3707–3727.

Surcel, M., M. Berenguer, I. Zawadzki, 2010: The Diurnal Cycle of Precipitation From Continental Radar Images and Numerical Weather Prediction Models. Part I: Methodology and Seasonal Comparison. *Mon. Wea. Rev.*, **In press.**

Wallace, J., 1975: Diurnal Variations in Precipitation and Thunderstorm Frequency over the Conterminous United States. *Mon. Wea. Rev.,* **103**, 406–419.